Journal of South American Earth Sciences 97 (2020) 102375

Contents lists available at ScienceDirect

Journal of South American Earth Sciences

journal homepage: www.elsevier.com/locate/jsames

Earthquake potential in Costa Rica using three scenarios for the central Costa Rica deformed belt as western boundary of the Panama microplate

Luis Alejandro Carvajal-Soto[a,*], Takeo Ito[b], Marino Protti[c], Hiroshi Kimura[a]

[a] Graduate School of Environmental Studies, Nagoya University, Faculty of Science, Faculty E, Building 4 F 407, 464-8601 Dero Town D2-2 (510), Chikusa-ku, Nagoya City, Japan

[b] Earthquake and Volcano Research Center, Nagoya University, Faculty of Science, Faculty E, Building 4 F 407, 464-8601 Dero Town D2-2 (510), Chikusa-ku, Nagoya City, Japan

[c] Observatorio Vulcanológico y Sismológico de Costa Rica (OVSICORI), Universidad Nacional de Costa Rica, 2386-3000 Heredia, Costa Rica

ARTICLE INFO

Keywords:
Central Costa Rica
Crustal deformation
Earthquake potential

ABSTRACT

The Central Costa Rica Deformed Belt (CCRDB) is a diffuse faulting area that represents the western border of the Panama Microplate. Using the Markov Chain – Monte Carlo method and under three scenarios of the spatial distribution of the CCRDB, we analyzed the inter-seismic crustal deformation in Costa Rica and its surroundings based on the results of the Global Navigation Satellite System (GNSS) observations for Costa Rica, Nicaragua, and Panama. We assumed that the observed inter-seismic crustal deformation on the surface is a result of the kinematic effects of the rigid tectonic blocks motion, the elastic deformation due to the block interface interactions and the internal strain inside of the tectonic blocks. Assuming that the seismic moment in the subduction and inland interfaces is accumulated only as an elastic strain and is then released co-seismically, the resulting seismic moment accumulated rates reflect the capacity for producing earthquakes $M_w > 8$ along the Cocos Plate convergence and earthquakes $M_w > 7$ along the inland interfaces. Although these are the values that the modeling outputs, limited historical data suggests that this earthquake potential might be overestimated, but the historical seismicity in Costa Rica is still short for disesteeming higher earthquake potential levels.

1. Introduction

Adamek et al. (1988) defined the Panama Microplate (PM) as a separate tectonic unit that overthrusts the Caribbean Plate (CA) in a northward direction, whose kinematics is associated by Montero (2001) with the subduction morphology of the Cocos Plate (CO) in the southwestern PM (Fig. 1). The CO segment subducting beneath Costa Rica along the Middle American Trench (MAT) has a convergence rate from 75 to 80 mm/yr relative to the CA motion (Argus et al., 2011). This subduction interface has produced several historical $M > 7$ earthquakes (Morales, 1985; Montero, 1986; Protti et al., 2013), and three morphotectonic domains of the oceanic crust have been identified on this interface (Barckhausen et al., 1998; Protti et al., 1994; Von Huene et al., 2000): the Cocos Ridge, the Seamount and the Smooth seafloor domains (Fig. 1). The subduction of the Cocos Ridge and the Seamount domain has had remarkable implications for the seismicity and crustal deformation of the upper plate (*e.g.,* Vanness et al., 1984; Protti et al., 1994; Fisher et al., 1998; LaFemina et al., 2009). In the northern PM, the PM-CA interaction takes place along the North Panama Deformed Belt (NPDB) (Silver et al., 1990) (Fig. 1), where the hypocenters of several earthquakes are found, suggesting overthrusting at this boundary (*e.g.,* Adamek et al., 1988). Based on the seismicity, Camacho et al. (2010) suggested the presence of a well-defined Wadati–Benioff zone and an active subduction interface along NPDB, where earthquakes $M \geq 7$ have been reported (*e.g.,* Camacho and Víquez, 1993; Goes et al., 1993; Suárez et al., 1995). Marshall et al. (2000), based on the seismic sequence ruptures in-between earthquake epicenters in the southwestern PM due to the CO subduction and in the northwestern PM due to CA subduction, concluded on the presence of an active tectonic link connecting these two tectonic edges. In the southeastern PM (Fig. 1), the interaction of the PM with the Nazca Plate (NZ) is a predominant sinistral slip boundary with an oblique convergence component along the South Panama Fracture Zone (SPFZ), characterized by a weak seismic interface (*e.g.,* Adamek et al., 1988; Moore and Sender, 1995).

The western PM boundary consists of the Central Costa Rica

* Corresponding author.
E-mail addresses: luis@seis.nagoya-u.ac.jp (L.A. Carvajal-Soto), takeo_ito@nagoya-u.jp (T. Ito), marino.protti.quesada@una.cr (M. Protti), kimura@seis.nagoya-u.ac.jp (H. Kimura).

https://doi.org/10.1016/j.jsames.2019.102375
Received 8 July 2019; Received in revised form 1 October 2019; Accepted 1 October 2019
Available online 04 October 2019

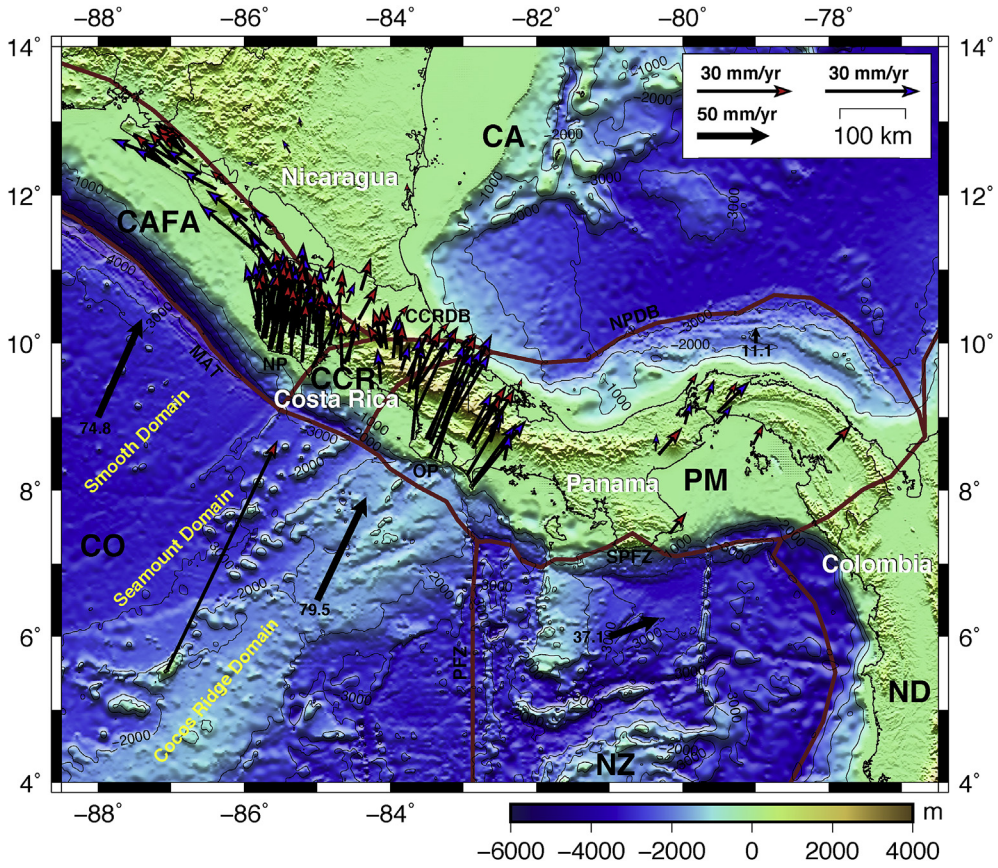

Fig. 1. Tectonic configuration around Costa Rica. Red arrows are observations processed in this study and blue ones are from previous studies (see Table S1), both relative to CA. Brown contours are block boundaries (*modified from* Bird, 2003; Marshall et al., 2000; Kobayashi et al., 2014). Black arrows are plate motions relative to CA (Argus et al., 2011). Velocities are given in mm a-1. Thin black contours are bathymetry according to ETOPO1 Model (Amante and Eakins, 2009). Subduction Domains are according to Von Huene et al. (2000). CO: Cocos Plate, CA: Caribbean Plate, PM: Panama Plate, NZ: Nazca Plate, ND: North Andes Block, CAFA: Central American Fore Arc Block, CCR: Central Costa Rica Block, MAT: Middle American Trench, NP: Nicoya Peninsula, OP: Osa Peninsula, CCRDB: Central Costa Rica Deformed Belt, NPDB: North Panama Deformed Belt, SPFZ: South Panama Fracture Zone and PFZ: Panama Fracture Zone.

Deformed Belt (CCRDB), the western extension of NPDB (Fig. 1). Montero and Dewey (1982) suggested a sinistral transcurrent fault system in the central zone of Costa Rica. Later, Montero (2001) described CCRDB as a wide deformation zone (herein called Central Costa Rica) formed by a complex faulting system, instead of a simple sinistral boundary. Several studies have been conducted on the presence of this complex tectonic interface (*e.g.,* Barboza et al., 1995; Protti et al., 1995; Quintero and Güendel, 2000), whose faulting and deformation pattern have been associated with the indentation of the shallow Cocos Ridge and roughness seamounts subduction (*e.g.,* Marshall et al., 2000; Montero, 2001). Inland faulting in CCRDB has produced several shallow destructive M > 6 earthquakes, such as the Cartago 1910 M 6.4 (Alonso-Henar et al., 2013), the Bajos del Toro 1911/1912 M 6.1 (Alvarado et al., 1988), the Orotina 1924 M 7.0 (Montero, 1999), the Damas 2004 M_w 6.4 (Pacheco et al., 2006) and the Cinchona 2009 M_w 6.2 (Barquero, 2009) earthquakes. As the limit of the western PM, CCRDB has an interface with the Central America forearc block (CAFA) (Fig. 1), where M > 6 earthquakes have been reported (*e.g.,* Linkimer et al., 2018).

Previous studies based on earthquake focal mechanisms, local faulting and geodesy, defined the boundaries of Central Costa Rica (CCR). Marshall et al. (2000) outlined the CCRDB zone through the evaluation of mesoscale fault outcrops in conjunction with earthquake focal mechanisms, indicating that this zone is dominated by a sinistral transtension across NE striking faults in the forearc. Marshall et al. (2000) also suggested that the central volcanic and back arcs are characterized by a dual pattern of dextral slip with NW shortening and sinistral slip with minor extension on NE striking faults. Based on the inversion of Global Navigation Satellite System (GNSS) observations and earthquake slip vectors, Kobayashi et al. (2014) suggested through the analysis of several kinematics models that the western PM edge can be conformed directly by the CAFA-PM boundary, without the presence of the CCRDB as a discrete block, indicating that CCRDB accommodates NW-SE extension. In addition, Montero and Rojas (2014) proposed a new boundary for the CCRDB zone, enhanced with the results from previous studies on the seismicity, seismotectonics, and the temporal evolution of the fault system (*e.g.*, Montero, 2001; Montero et al., 2013).

In this study, we analyze the inter-seismic crustal deformation in Costa Rica and its surroundings based on GNSS observations under three kinematic models that include different coverages of the CCRDB zone as the rigid CCR block, which are inferred as follows: Model 1 (Fig. 2a) from the outlined CCRDB zone described by Marshall et al. (2000), Model 2 (Fig. 2b) from results of the best kinematic model by Kobayashi et al. (2014), and Model 3 (Fig. 2c) from the enhanced CCRDB zone defined by Montero and Rojas (2014). We assume that the observed inter-seismic crustal deformation on the surface results from: i. The kinematic effects of rigid tectonic block motions of CCR, PM, CO, CA, CAFA, and NZ; ii. The elastic inter-seismic deformation due to the block interactions on the subduction and inland interfaces; and iii. The elastic deformation owing to the internal strain inside of each tectonic block. For the first time, we employ the Markov Chain Monte Carlo (MCMC) method in order to approximate the solution of the kinematics and the crust deformation patterns in Costa Rica and its surroundings. Compared with previous studies, we double the number of observation sites in CCR for an improved constraint in this target area. We present for all models a detailed description of the total budget of the inter-seismic crustal deformation and we select the best model in consistency with faulting and seismicity behaviors. For the best model, we integrate the results of the slip deficit rates on the plate interfaces with the local historical seismicity in order to estimate the earthquake potential in Costa Rica.

2. Geodetic data and velocity field

Geodesy is helpful for studying tectonic plate motions and crustal

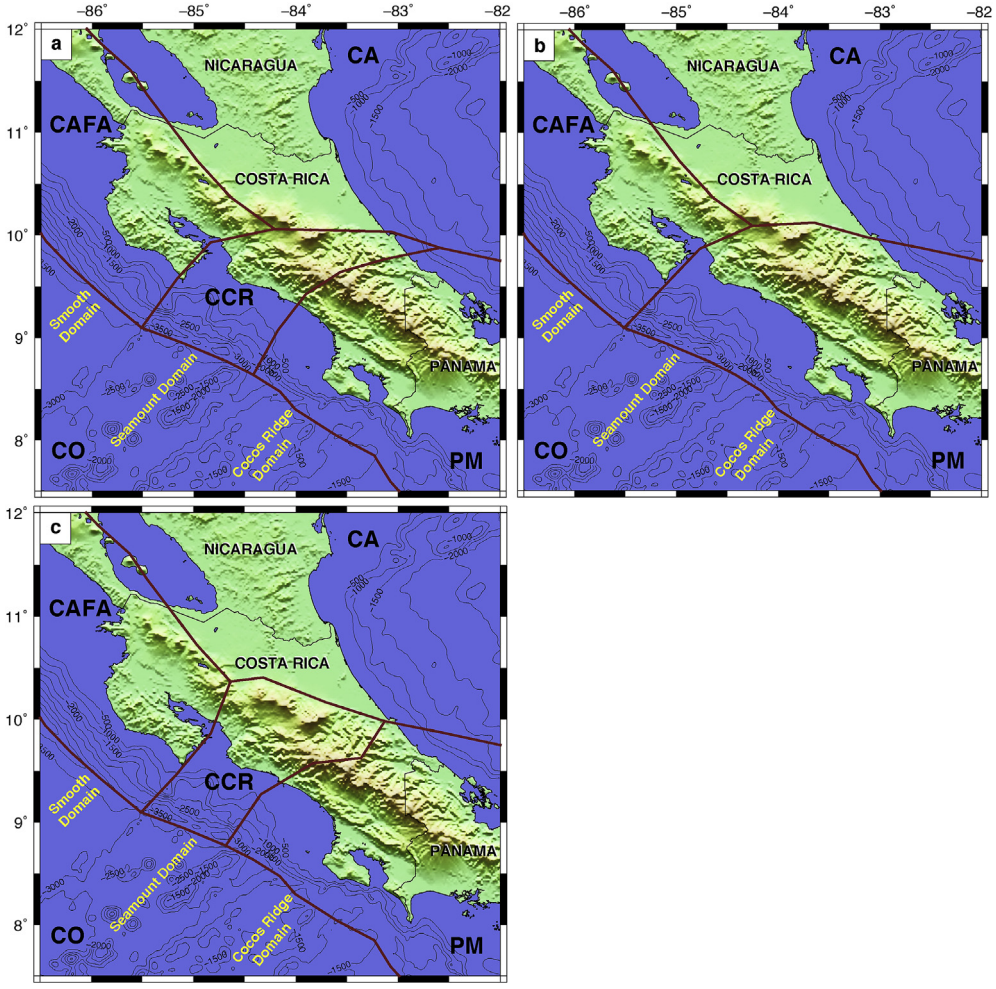

Fig. 2. Geometry of model blocks: a. Model 1, b. Model 2 and c. Model 3. Brown lines are the block boundaries. Black thin contours are bathymetry according to ETOPO1 Model (Amante and Eakins, 2009). Subduction Domains are according to Von Huene et al. (2000). CO: Cocos Plate, CA: Caribbean Plate, PM: Panama Plate, NZ: Nazca Plate, CAFA: Central American Fore Arc Block, CCR: Central Costa Rica Block.

deformation (*e.g.,* Argus and Heflin, 1995) because it enables monitoring the crust during inter-seismic, co-seismic and post-seismic deformations and slow slip events (*e.g.*, Bürgmann and Thatcher, 2013; Klein et al., 2018). Currently, Costa Rica allocates a heterogeneous distributed GNSS/GPS network that is more densely available in northwestern Costa Rica on the Nicoya Peninsula (NP) than in the northern, Central, and southeastern Costa Rica.

Fig. 1 shows the distribution of the GNSS network sites in Costa Rica, Nicaragua and Panama. In total, this study includes 76 continuous observation sites (Table S1), providing data from January 2004 to May 2017, available from *Observatorio Vulcanológico y Sismológico de Costa Rica–Universidad Nacional*, *UNAVCO*, and *Nevada Geodetic Laboratory*. Forty-five sites are located in Costa Rica, including seven observation sites inside the target area in CCR and northern Costa Rica (sites not previously used in related studies such as LaFemina et al., 2009 and Kobayashi et al., 2014). In addition, there are 14 sites in Nicaragua, 8 in Panama and 9 in the Caribbean and Pacific islands (7 sites in CA and 2 sites in NZ; not shown in Fig. 1).

First, GNSS data with a minimal spanning of 2.5 years were selected (*e.g.,* Blewitt and Lavallée, 2002) and processed in conjunction with 9 IGS sites (Dow et al., 2009) for a regional constraint using the Bernese 5.2 software developed at the Astronomical Institute of the University of Bern.

In order to obtain a highly precise velocity field of crustal deformation, we eliminated non-tectonic effects as seasonal components (annual or semi-annual) and artificial steps, which were attributed to unknown phase center offsets after maintenance works (found from the RINEX files inspections). In addition, we removed tectonic offsets due to earthquakes that could have generated displacements larger than 5 mm following the Okada criterion (Okada, 1995). The formulation of the nonlinear fitting process applied is as follows:

$$u(t) = a + bt + c\sin(2\pi t) + d\cos(2\pi t) + e\sin(4\pi t) + f \cos(4\pi t) + \sum_{i=1}^{N} g_i H(t - t_i) + \sum_{j=1}^{E}\left[h_j H(t - t_j) + k_j \ln\left(1 + {t_j}/{\tau_{as_j}}\right) + l_j\left(1 - \exp\left(-{t_j}/{\tau_{ve_j}}\right)\right)\right] \quad (1)$$

where $u(t)$ is the time series of displacement; a and b are the secular linear trend parameters; and c, d, e, and f are the annual and semi-annual seasonal parameters. g_i, h_j, k_j, and l_j are the offsets parameters at the occurrence times t_i and t_j for N number of artificial offsets and E number of earthquake offsets. H represents the Heaviside function, and τ_{as_j} and τ_{ve_j} are the nonlinear parameters of the constant decay time for after slip and viscoelastic relaxation, respectively.

The observed velocity field (76 sites) based on ITRF 2008 (Altamimi et al., 2011) was combined with the results reported by Kobayashi et al. (2014) (63 sites, including 42 additional sites in Costa Rica, 10 sites in Nicaragua, and 11 additional sites in Panama) based on ITRF 2005 (Altamimi et al., 2007) which were transformed to ITRF 2008 (Table

S1). In Fig. 1, the CA motion was fixed using a priori Euler pole information (Argus et al., 2011).

As in previous studies (*e.g.,* LaFemina et al., 2009; Kobayashi et al., 2014), the observed velocity field in Costa Rica suggests that the inter-seismic crustal deformation is mainly arranged in three groups (Fig. 1): 1) Northwestern Costa Rica is dominated by a northward deformation with rates up to 25 mm/yr, rotating and decreasing up to 12 mm/yr northwestward following CAFA. 2) Southeastern Costa Rica shows deformation to northeastward up to 40 mm/yr (opposite E–W motion in comparison to northwestern Costa Rica). 3) CCR is characterized by a diffuse deformation pattern, mainly oriented to northward with deformation rates up by half of those observed in northwestern and southeastern Costa Rica.

3. Block model boundaries

We analyzed a series of three kinematic models (Fig. 2) for CCR, following the boundaries inferred from Marshall et al. (2000) (Model 1), Kobayashi et al. (2014) (Model 2), and those suggested by Montero and Rojas (2014) (Model 3), which were well-described by Rodriguez (2017). Only Model 2 contained boundaries evaluated by geodetic techniques as in this study. Furthermore, in this study, we included additional sites to constrain the CCR block. The boundaries of the main plates, CO, CA, and NZ, were according to Bird (2003). The CAFA–CA boundary was the trace of the Central America forearc (*e.g.,* Kobayashi et al., 2014) and the boundaries of the CCR block are described in Table S2 and Fig. S1.

4. Kinematic model analysis

The geometry of the plate interface of the subducted CO plate was modeled with the Slab2.0 Model (Hayes et al., 2018), and the subducted southern edge of the CA plate along the NPDB was inferred from Protti and Schwartz (1994), Camacho et al. (2010) and Lücke and Arroyo (2015). For all models, the inland plate interfaces were projected as vertical boundaries up to 20 km in depth, consistent to a bottom depth level of 90% of the accumulative distribution of the inland seismicity (*e.g.,* Tanaka, 2004; Cho and Kuwahara, 2013).

We considered that the observed crustal deformation resulted from the inter-seismic deformation is produced by i) rigid block kinematics (*e.g.,* Sella et al., 2002), ii) elastic deformation due to the coupling effect at I number of block interfaces (*e.g.,* Nishimura, 2014), and iii) deformation owing to the internal strain in each block as a continuous function within the observation network, assuming a uniform strain rate field (*e.g.,* Shen et al., 1996) (Fig. 3).

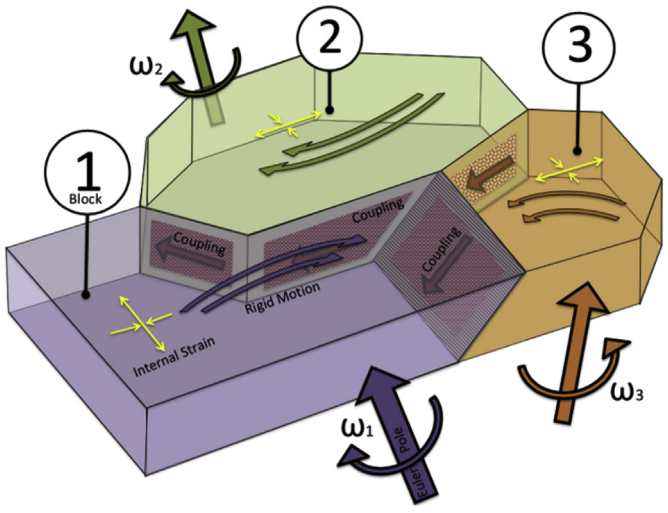

Fig. 3. Schematic visualization of the kinematic of tectonic blocks.

The rigid block kinematics V_{ik}^{Rigid} inside of a block is determined by the cross product of a position r_k and the Euler pole ω_i of the block:

$$V_{ik}^{Rigid} = \omega_i \times r_k \tag{2}$$

The relative velocity V_{ijl} along an interface r_l of two rigid blocks in motion (ω_i and ω_j) is determined as follows:

$$V_{ijl} = (\omega_i - \omega_j) \times r_l \tag{3}$$

Having the relative velocity on a plate interface V_{ijl}, one can calculate the slip deficit rate SDR_{ijl} in the boundary between blocks in motion due to the coupling effect C_l as follows:

$$SDR_{ijl} = C_l V_{ijl} \tag{4}$$

The elastic deformation due to the slip deficit $V_{ijl}^{E.Interfaces}$ in block interfaces and the elastic deformation due to the internal strain $V_{ik}^{E.\,Internal}$ are determined by the Green's functions G_{kl} and the horizontal strain tensor $\hat{E}_i$, respectively, where the $\hat{e}$ components are Cauchy's strain tensors, and Δ_{xi}, and Δ_{yi} are the vector components of r'_k, which represents the distance of a point r_k relative to the center of the spatial distribution of the observation network.

$$V_{ijk}^{E.Interfaces} = G_{kl}\, SDR_{ijl} \tag{5}$$

$$V_{ik}^{E.Internal} = \hat{E}_i r'_k = \begin{pmatrix} \hat{e}_{xx} & \hat{e}_{xy} \\ \hat{e}_{yx} & \hat{e}_{yy} \end{pmatrix} \begin{pmatrix} \Delta_{xi} \\ \Delta_{yi} \end{pmatrix} \tag{6}$$

In order to approach the observed crustal deformation d_k, we combine the previous equations as follows:

$$d_k^{Cal} = V_{ik}^{Rigid} + V_{ijk}^{E.Interfaces} + V_{ik}^{E.Internal} = \underline{\omega_i} \times r_k + \sum_{l=1}^{I} G_{kl}\, \underline{C_l}(\underline{\omega_i} - \underline{\omega_j}) \times r_l + \underline{\hat{E}_i} r'_k \tag{7}$$

Since the calculation of the crustal deformation d_k^{Cal} requires non-linear solutions of a high-dimensional system (unknown parameter underlined in (7)) with a limited number of constraints, we adopted for the solution of this formulation the MCMC method introduced by Metropolis et al. (1953) and estimated the probability density function of the unknown parameters for the calculation of confidence interval plots. The Markov chain provides a sequence of samples from a non-normal distribution, which depends on the current state of the chain. The Monte Carlo integration provides an adequate scope for the realistic statistical modeling used for approximating the expectations in our formulation (*e.g.,* Gilks et al., 1996). We followed the procedure defined in Kimura et al. (2019) for the calculation of the crustal deformation (equation (7)) using the MCMC algorithm.

Our MCMC algorithm explores randomly the parameters contained in (7), constructing a chain, where every new set of approximations is accepted or rejected using the Metropolis–Hastings algorithm (*e.g.,* Robert and Casella, 2004). The initial transient phase (burn-in) of iterations was discarded in order to maintain an approximately stationary realization from the marginal posterior distribution of interest (*e.g.,* Liu et al., 2014). A complete explanation about the MCMC method applied for crustal deformation in southwest Japan can be found in Kimura et al. (2019).

Table 1 shows the calculation settings of the application of the MCMC method in this study.

5. Results and discussion

After the MCMC calculations, we obtained for the three models the characteristics of the rigid motion and the inter-seismic elastic deformation due to the coupling effects on the block interfaces and the internal strain inside the blocks. The results of the observed velocity field and calculations for the horizontal and vertical components are shown in Figs. S2 and S3, respectively. The calculations in Model 1 and

Table 1
Calculation settings for MCMC method.

MCMC Calculation Settings	
Item	Initial value or setting
Initial Euler Poles	Estimated as rigid block rotations from GNSS velocities
Initial Slip deficit due coupling	Uniformly distributed random value (0–1)
Initial Strain tensor	Uniformly distributed random value ($-0.5 - 0.5$) x 10^{-10}
Markov Chain	1.500.000
Burn-In	20%

Model 3 present fewer residuals in comparison to those for Model 2 (for the residuals, see Figs. S4 and S5) and fewer residuals than previous studies conducted in the region (*e.g.,* LaFemina et al., 2009; Kobayashi et al., 2014). We presented for each model the results of the total displacement budget relative to the CA motion, based on the contribution on the surface of the rigid kinematic motion and the elastic deformation due to the block interface interactions and the internal strain inside of blocks.

5.1. Block rigid kinematics

The rigid motion of each block is described through the results of the Euler pole vectors and angular rates relative to the stable CA. Table 2 lists the results of Euler poles and its covariance matrix for each block in each model and Figs. S6–S8 show the pole positions. The estimated rigid motion of CAFA presents similarities in all models, characterized by a sliver scape with a counterclockwise rotation that shows a right lateral strike-slip motion of 9–16 mm/yr (northwestward) in agreement with the focal mechanisms pattern of seismicity along the CAFA–CA boundary (*e.g.,* DeMets, 2001; LaFemina et al., 2002). Correcting for CA motion, the rigid motion dominates the inner forearc displacement on-shore of the CAFA block, reaching more than 60% of the total displacement budget with an exception in Nicoya Peninsula, the closest land to MAT, where the relative contribution of the rigid motion represents less than 30% in all models (Figs. S9, S10, and S11 for Models 1, 2, and 3, respectively).

In all models, the PM block shows a counterclockwise rotation, producing northeastward collision to CA with a relative convergence rate at the northeastern PM reaching 7.7 ± 0.3 mm/yr and a predominant left lateral strike motion up to 24.5 ± 0.4 mm/yr along the boundary with NZ. The northwestern PM in Models 1 and 3 shows collision along the western NPDB. This collision is consistent with the focal mechanism solution of the 1991 Mw 7.7 Valle de la Estrella Earthquake (*e.g.,* Protti and Schwartz, 1994), while Model 2 shows a null pattern of motion at the same zone. The relative contribution of the rigid motion in the displacement budget of the PM is gradually increasing from less than 15%–90% from the western PM to eastward. The relatively low contribution of the rigid motion in the western PM and southeastern CAFA is due to the subduction of CO, and this effect is discussed in section 5.2.

For CCR, rigid kinematics represents less than 40% of the total displacement budget. The results for Model 1 and Model 3 show clockwise motions. However, due to the counterclockwise rotation of CAFA, the results of the normal rate at the CCR–CAFA boundary suggest a relative extensive pattern at the northeastern segment of this boundary, reaching 4.1–4.4 mm/yr in these two models (Figs. S9 and S11). Nevertheless, the PM in Model 2 shows the opposite (counterclockwise) kinematics with the higher extensive rates of 11.6–12.2 mm/yr along this interface (Figs. S10 and S12). The clockwise motion reflected in Models 1 and 3 suggests a relative extensive pattern of 3.1–9.3 mm/yr in Model 1 (Figs. S9 and S12) and 3.8–8.5 mm/yr in Model 3 (Figs. S11 and S12) along the CCR–PM boundary with progressive crescent rates from northwestern PCT to off-shore. We infer that the extensive patterns presented in CCR in Models 1 and 3 are consistent with transtension across NE striking faults reflected by mesoscale faults in the on-shore inner forearc (Marshall et al., 2000).

The strike velocities along the CCR–CAFA boundary in Model 1 suggest a relative left lateral strike-slip motion with progressive crescent rates from off-shore to the inner forearc of 2.1–3.9 mm/yr (Fig. S12). However, contrary to the Model 1, Models 2 and 3 suggest right lateral motion with relative rates smaller than 2.1 mm/yr in Model 3 and higher than 5.1 mm/yr in Model 2 (Fig. S12). The focal mechanisms of destructive earthquakes, such as those reported for the 1924 M 7.0 Orotina earthquake (Montero, 1999), show left lateral behavior close to the trajectory of CCR–CAFA boundary, as it is indicated by the kinematics in Model 1 (*e.g.,* Jacob et al., 1991; Montero, 1999) (Fig. S12). The relative strike motion along the CCR–PM boundary shows a left lateral pattern in all models, reaching progressive crescent rates from off-shore to back arc of 0.9–4.2 mm/yr for Model 1 and 2.9–6.1 mm/yr in Model 3 (Figs. S11 and S12). An extensional pattern in combination with a relative left lateral striking motion in the forearc along the CCR–PM boundary, as shown in Models 1 and 3, is consistent with focal mechanisms of events reported close to this boundary, with normal components and left lateral slip motion, as in the case of the 1983 M 6.1 earthquake and the induced seismicity reported after the 1991 Mw 7.7 Valle de la Estrella Earthquake (*e.g.,* Protti and Schwartz, 1994; Boschini et al., 1988; Barquero and Rojas, 1994; Fernández et al., 1996; Pacheco et al., 2006) (Fig. S12).

Model 2 shows extensive patterns at the CCR–CA boundary that progressively increase westward with relative dip velocities of 0.4–1.3 mm/yr (Figs. S10 and S12). In Models 1 and 3, these two blocks collide with progressively increasing relative rates of 0.2–2.6 mm/yr in

Table 2
Estimated Euler Pole for models relative to Caribbean Plate.

Euler Pole Results										
Model	Block	Latitude (°)	Longitude (°)	Angular rate (° Myr^{-1})	*xx*	*xy*	*xz*	*yy*	*yz*	*zz*
					Covariance Matrix (10^{-8} rad^2 Myr^{-2})					
1	NZ	53.88	−110.88	0.35	0.05	0.11	0.02	1.15	0.17	0.09
	CAFA	8.00	−87.61	1.41	7.21	−64.58	12.35	595.17	−114.49	22.07
	CCR	−10.05	96.67	2.25	2.37	−24.61	4.53	262.60	−48.68	9.18
	PM	11.33	−84.69	0.64	1.36	−7.11	1.13	37.98	−6.02	0.98
2	NZ	56.15	−111.72	0.34	0.05	0.08	0.00	1.03	0.12	0.08
	CAFA	8.93	−86.80	1.99	0.47	−3.72	0.83	54.36	−11.72	2.56
	PM	9.95	−83.19	0.92	0.34	−2.29	0.31	16.44	−2.14	0.33
3	NZ	52.08	−110.28	0.35	0.04	0.06	0.00	0.90	0.11	0.07
	CAFA	8.88	−86.84	2.06	0.75	−8.72	1.81	110.57	−22.99	4.79
	CCR	−10.38	96.53	2.00	5.42	−55.17	10.17	577.46	−107.14	20.01
	PM	12.15	−86.07	0.51	0.69	−3.78	0.59	21.56	−3.35	0.55

Model 1 (Figs. S9 and S12) and 1.7–3.9 mm/yr in Model 3 (Figs. S11 and S12). Along this interface, the strike relative motion is almost zero in Models 1 and 2, whereas Model 3 shows right lateral motions with relative rates higher than 1.3 mm/yr. Taking into account the presence of reverse faults in northeastern CCR, we infer that the compressive patterns shown in Models 1 and 3 reflect more consistencies than the extensive pattern in Model 2 (Denyer et al., 2003) (Fig. S12).

5.2. Elastic deformation due to block interactions

In our models, the elastic inter-seismic deformation is produced by interactions along block interfaces. In all models, the high northeastward convergence rate of CO, combined with nucleation of high or moderate coupling ratios, results in compressive patterns in CAFA, CCR, and the western PM. Although we considered the effect of this coupling along the inland interfaces, elastic deformation is governed by the subducting interface of CO, even in places located close to inland boundaries and back arc zones of CCR and the western PM. Figs. S13 and S14 show the spatial distribution of the coupling for the subduction and inland interfaces, respectively. Fig. S15 presents the results of 90% of confidence interval for coupling ratio for both block interface types.

Our calculations show, in all models, high coupling ratios along the CO subduction interface in southeastern CAFA, close to Nicoya Peninsula. All models present similar patterns of the coupling ratios. The maximum coupling ratio is 0.98 ± 0.01 in Model 1, 0.95 ± 0.03 in Model 2, and 0.98 ± 0.02 in Model 3. In the surrounding zones, moderate coupling ratios between 0.70 and 0.85 are reached for all models (Fig. S13). Likewise, the maximum coupling ratios converge more in the subduction interface of CO in southwestern PM, close to Osa Peninsula, than in NP; the highest coupling ratio is 0.99 ± 0.01 in all models, with greater coverage in Model 2 than in Models 1 and 3 (Fig. S13). These high coupling ratios resulted in northeastward inter-seismic elastic deformations on the surface in southeastern CAFA and southwestern PM that reach rates higher than 20.0 mm/yr in NP and 35.0 mm/yr in OP, representing more than 70% and 85% of the total deformation budget, respectively (Figs. S16–S18). Historical seismicity M > 7 provides evidence of asperities in these two zones (*e.g.,* Montero, 1986; Morales, 1985; Protti et al., 1996; Protti et al., 2001). The highest inter-seismic elastic deformation resulted in the overriding PM in southeastern Costa Rica as a consequence of the compressive pattern produced by the locked subduction of the wide buoyancy Cocos Ridge domain (Montero, 1994). In northeastern Costa Rica, although our models show an unclear pattern of coupling ratios for the PM–CA subduction interface (Fig. S13), the northeastward inter-seismic deformation rates are lower than 12.0 mm/yr. These results are not well constrained in our models due to the sparse observation network, but they do agree with the presence of the reverse faults and low deformation rates reported by Suárez et al. (1995).

Several studies have been conducted in Costa Rica and its surroundings for the evaluation of the coupling due to the subduction of the CO; showing more moderate coupling ratios (0.5–0.65) in NP (*e.g.,* Kobayashi et al., 2014; LaFemina et al., 2009; Norabuena et al., 2004), and OP (*e.g.,* Kobayashi et al., 2014; LaFemina et al., 2009). Our results show similar distribution of high coupling ratios to Feng et al. (2012) and a scenario in Protti et al. (2001) (> 0.9) in NP. The main differences are owing to 1. The number and distribution of the GNSS observation sites inverted in this study is higher on the target area; 2. Different geometry models of the subduction interfaces (*e.g.,* Kobayashi et al., 2014; LaFemina et al., 2009; Norabuena et al., 2004); 3. The coupling behavior was not constrained as it was controlled in best models previously suggested (*e.g.,* Kobayashi et al., 2014; LaFemina et al., 2009; Norabuena et al., 2004); 4. The MCMC method calculated all the parameters simultaneously from the horizontal (trench parallel and normal) and vertical velocity field, while studies as Norabuena et al. (2004) made inversion of the Euler poles and elastic strain not simultaneously; and 5. We applied, for the first time, the MCMC method for the parameters calculation in this study area, and compare to previous studies analyzed using DEFNODE (*e.g.,* Kobayashi et al., 2014; LaFemina et al., 2009) our results reflect less residuals (Figs. S4 and S5).

Inter-seismic elastic deformation in CCR represents more than 60% of the total displacement budget in this block. Moderate coupling ratios are shown in Models 1 and 3 for CCR, with maximum ratios in southeastern Nicoya Peninsula reaching 0.68 ± 0.03 and 0.65 ± 0.08, respectively, and low ratios in the surrounding zones (0.02–0.40 in both models; Fig. S13). Model 2 reflects higher coupling ratios in comparison to Models 1 and 3, reaching 0.79 ± 0.05 in Central Pacific Costa Rica. We attributed the high elastic deformation calculated in Model 2 to the counterclockwise rigid motion of the western PM, where the high coupling ratio in the subduction interface is a neutralization response against the counterclockwise rigid motion. Nevertheless, this scenario of high coupling ratios cannot be explained by the historical seismicity (as it can be explained in the Nicoya or Osa Peninsula) due to the absence of earthquakes on this interface with a magnitude higher than M_w 7 (Protti et al., 1995).

Model 1 and model 3 offer a driving mechanism that partially agrees with LaFemina et al. (2009), where the sliver motion of CAFA was attributed to the oblique convergence of CO and the contribution of the Cocos Ridge subduction. Instead, our results suggest that this driving motion is the result of the oblique convergence of CO and the contribution of the collision between the CCR–CAFA blocks in southwestern CCR, as a consequence of the Seamount Domain subduction beneath CCR and the resulting clockwise motion of the CCR block. Nevertheless, Protti et al. (2001), suggest that the subduction beneath off Central Costa Rica is weak due to the seamounts acting as small asperities that break often with moderate events, therefore, does not transfer significant deformation to the upper plate in Central Costa Rica, where the stresses cannot propagate far on inland through the faulting zone. The Cocos Ridge domain is activated northeastward directly to the PM, resulting in a different kinematic behavior (counterclockwise rotation), which is observed in all our models and it could result unrealistic to expect a strong contribution for the sliver motion of CAFA.

Although the vertical velocity field in Costa Rica shows high residuals, the inter-seismic elastic deformation in the on-shore area exceeds 11 mm/yr of subsidence in NP and 14.0 mm/yr in OP in all models. Southeastern Costa Rica has the highest uplift elastic deformation, more than 3 mm/yr in all models (Figs. S19–S21). The higher uplift reflected in southeastern Costa Rica is a dual effect produced by the subduction of the Cocos Ridge on the CO-PM interface and the compressive domain produced by the back arc thrust effect of the CA–PM subduction in northeastern Costa Rica (*e.g.,* Montero et al., 1992; Suárez et al., 1995). The interseismic deformation along the Pacific coast and northeastern Costa Rica is mainly elastic deformation and is recovered with every large earthquake (Protti et al., 2001). The co-seismic deformation is viscous-elastic deformation where the viscous part remains as permanent deformation bringing up NP, OP and the coast region of northeastern Costa Rica and produces permanent subsidence along the Nicoya and Dulce gulfs (Protti et al., 2001).

5.3. Elastic deformation due the internal strain

In comparison to the rigid motion and the elastic deformation produced by interactions along block interfaces, we found in all models that a small fraction of the total inter-seismic displacement budget is due to the effect of the internal strain (less than 1% for CCR, CAFA, and CO, and less than 10% for PM and NZ). Table S3 contains the results of maximum, minimum, and shear strains and their axes orientations for all models.

The principal strain axes in CAFA, result in Models 2 and 3 in a compressive pattern northwestward and an extension pattern northeastward, with higher strain values in Model 3, up to 0.39 ± 0.16 nanostrain/yr for contraction and up to 0.28 ± 0.17 nanostrain/yr for

extension. In comparison to the other models, Model 1 reflects different strain axes orientation, characterized by compression of 0.55 ± 0.24 nanostrain/yr in the east–west direction and extension of 0.23 ± 0.1 nanostrain/yr in the north–south direction (Fig. S22).

In the PM block, the orientation of principal strain axes shows similarities in Models 2 and 3; north–northeastward for compression and west–northwestward for extension. However, the strain values differ; Model 2 shows maxima strains of 0.68 ± 0.23 nanostrain/yr for contraction and 1.62 ± 0.54 nanostrain/yr for extension. The highest value for extension in Model 2 is influenced by the presence of more observation sites that constrain the western PM; observation sites in the western PM show short east components of deformation, while more eastward observation sites show high east component of deformation. Model 1 also shows a different pattern of principal strain axes in comparison to other models, with a north–south axis of 0.11 ± 0.09 nanostrain/yr for compression and an east–west axis of 0.83 ± 0.25 nanostrain/yr for extension (Fig. S22).

Our results of the internal strain in CCR do not differ significantly, with regard to the orientation of the strain axes between models that contain this block. However, both principal strain axes in Model 3 show a northeastward compression of 0.52 ± 0.13 nanostrain/yr and a northwestward compression of 0.11 ± 0.12 nanostrain/yr. On the contrary, Models 1 and 2 show northeastward compression of 0.59 ± 0.18 nanostrain/yr and 0.73 ± 0.21 nanostrain/yr, and northwestward extension of 0.69 ± 0.17 nanostrain/yr and 0.24 ± 0.21 nanostrain/yr, respectively (Fig. S22). The consequent shear strain in all models for CCR is consistent with the inland faulting pattern and the focal mechanisms of the inland seismicity, dominated by strike-slip events (*e.g.,* Marshall et al., 2000; Arroyo et al., 2014; Fernández et al., 1996; Fan et al., 1993; Montero, 2001; Denyer et al., 2003; Barquero and Rojas, 1994). Nevertheless, Model 1 is in concordance with the extensive pattern defined through northeast striking faults in CCRDB (Marshall et al., 2000; Denyer et al., 2003).

For models that contain the CCR block, we compared the average historic seismic moment release rate ($M_o^{(\text{released})}$) produced inside the seismogenic volume of the block, with the minimum scalar moment rate resulting from the principal surface strain rates ε_1 and ε_2 $M_o^{(\min)} = 2\mu HA\ Max(|\varepsilon_1|, |\varepsilon_2|, |\varepsilon_1 + \varepsilon_2|)$) obtained from the geodetic observations (Savage and Simpson, 1997). The seismogenic volume $V = AH$ is based on the local seismicity catalog of *Observatorio Vulcanológico y Sismológico de Costa Rica–Universidad Nacional,* where A is the area defined as the CCR block edges minus an offset of 5 km in order to avoid contamination from the seismicity produced in the block interfaces. H corresponds to the bottom depth level of 90% of the accumulative distribution of the inland seismicity (*e.g.,* Tanaka, 2004; Cho and Kuwahara, 2013) and μ is the rigidity (32 GPa). This comparison shows that Models 1 and 3 reflect a $M_o^{(\text{released})}/M_o^{(\min)}$ ratio of 2.11 and 2.61, respectively (Fig. S23). A better balance between the historic seismic moment release rate and the minimum scalar moment accumulation rate is obtained from Model 1.

5.4. Slip deficit and earthquake potential in Costa Rica

Model 1 is more consistent with the criteria presented in session 5.1, 5.2, and 5.3 (Table 3). From this model, we obtained the slip deficit rates on the block interfaces (equation (4)) based on the interaction between the rigid motions of two blocks defined by their Euler poles and the coupling ratio in the boundary interface (Figs. 4 and 5). Taking into account the slip deficit rate on a certain boundary, we estimated the seismic moment accumulation rate as $\bar{M}_o = \mu \text{A}\ SDR$, where μ is the rigidity (32 GPa), and A and SDR represent the locked area and the slip deficit rate on the block interface, respectively. We compiled a list of M > 6 earthquakes from previous studies in order to calculate the total seismic moment released from the year 1798 for subducting earthquakes and M > 5.5 earthquakes from the year 1772 for inland earthquakes (*e.g.,* Peterson and Seno, 1984) (Tables S4 and S5, respectively). We assumed that the seismic moment in a whole segment or sub-fault is accumulated only as elastic strain and is released coseismically. This assumption represents an upper limit of the earthquake potential since additional effects may contribute to the release of accumulated slips, such as the post-seismic deformation, plastic deformation, and the occurrence of slow slip events (*e.g.,* Jiang et al., 2012) (see discussion about the contribution of slow slip events in NP and surroundings identified in previous studies below).

Outside of the CCR block, three zones reflect a high concentration of coupling ratios that produce high slip deficit rates due to the CO–CAFA convergence (Fig. 4). In the NP, a locked area of ~5400 km^2 shows a weighted average of slip deficit rate of 62.1 ± 2.0 mm/yr, equivalent to a seismic moment accumulation rate of 10.7 ± 0.35 × 10^{18} J/yr (Fig. S24 and Tables S6 and S7). Based on Hanks and Kanamori (1979), the historical seismicity reaches a total release seismic moment rate of ~3.65 × 10^{18} J/yr, resulting in a seismic moment deficit rate of 7.05 ± 0.35 × 10^{18} J/yr, enough deficit to produce a M_w 8.1 earthquake every 225 ± 11 years.

Close to the previously described zone, a smaller zone in northern NP shows a moderate coupling ratio of 0.48 ± 0.07 consistent with a concentration of asperities (Fig. 4). This subducted zone reflects a slip deficit rate of 35.61 ± 4.81 mm/yr, representing a seismic moment accumulation rate of 13.45 ± 1.82 × 10^{17} J/yr (Fig. S25 and Tables S8 and S9). The largest reported historical earthquake in this zone was in 1950 with an M 7.7 (~3.98 × 10^{20} J) (Table S9); it resulted from a recurrence period of 296 ± 41 years for M_w 7.7 earthquakes or 53 ± 7 years for M_w 7.2 earthquakes.

If previous two zones being released as a single segment, a locked area of ~7600 km^2 and a weighted average of slip deficit rate of 49.9 ± 2.41 mm/yr, could represent a seismic moment accumulation rate of 12.1 ± 0.58 × 10^{18} J/yr (Fig. S26 and Tables S10 and S11). Both groups of historical seismicity released a total seismic moment rate of ~6.59 × 10^{18} J/yr, keeping a seismic moment deficit rate of 5.51 ± 0.58 × 10^{18} J/yr, enough deficit to produce a M_w 8.1 earthquake every 288 ± 31 years.

On the CO–CCR subduction interface in southeastern NP, the resulted coupling ratios reach 0.68 ± 0.03, consistent with the evidence of asperities based on historical earthquakes (Table S4). We evaluated an area of ~4100 km^2 showing a weighted average of slip deficit rate of 32.23 ± 3.9 mm/yr, equal to a seismic moment accumulation rate of 42.06 ± 4.16 × 10^{17} J/yr (Fig. S27 and Tables S12 and S13). Historical seismicity discloses a total release seismic moment rate of ~15 × 10^{17} J/yr, maintaining a seismic moment deficit of 27.06 ± 4.16 × 10^{17} J/yr equivalent to a M_w 7.4 earthquake every 52 ± 8 years. This recurrence interval is similar to a period of 54 ± 4 years proposed for earthquakes with magnitude 7.0 (based on not complete enough earthquake catalogs) in Protti et al. (1995). We suggest that the contribution of slow slip events in the entrance of the Nicoya gulf and the aseismic creep along the gap between seamounts reflects the differences between these two earthquake magnitudes for these similar recurrence intervals (see discussion about the contribution of slow slip events in this segment below).

High slip deficit rates reflected in high coupling ratios expose a locked area of ~16,500 km^2 in southeastern Costa Rica (CO–PM), beneath the Osa Peninsula (Fig. 4). The weighted average of the slip deficit rate in this zone is 62.01 ± 5.02 mm/yr, equivalent to a seismic moment accumulation rate of 32.83 ± 2.66 × 10^{18} J/yr (Fig. S28 and Tables S14 and S15). In comparison with NP, in OP, the historical seismicity (Table S15) reveals a wider zone of asperities that releases a seismic moment rate of ~8.11 × 10^{18} J/yr, maintaining a seismic moment deficit of 24.72 ± 2.66 × 10^{18} J/yr. This high seismic moment deficit rate is comparable to a M_w 8.3 earthquake every 128 ± 14 years. Nevertheless, records of historical earthquakes along this segment did not show earthquakes M_w > 8, suggesting that additional tectonic effects may be contributing to the release of accumulated slips, such as the post-seismic deformation, the shortening along the forearc

Table 3
Criterions for selection of the best model.

Criterions for Best Model Selection			
Criterion Adopted	Model 1	Model 2	Model 3
Less residuals between OBS and CAL of the ISD in the surface.	Yes	Not	Yes
RM of NW PM reflects relative collisions with CA consistent with FMS of Mw 7.7 VE EQ (*e.g.,* Protti and Schwartz, 1994).	Yes	Not	Yes
CCR shows an extensive pattern in consistency with transtension across NE striking faults (*e.g.,* Marshall et al., 2000).	Yes	Not	Yes
CCR-CAFA interface shows relative LLM consistent with FMS of the 1924 M 7 OR EQ and the 1990 M 5.7 PN EQ (*e.g.,* Jacob et al., 1991; Fernández, 1996) and consistent with LLM faults as BF, TF and LGF (Denyer et al., 2003).	Yes	Not	Not
CCR-PM interface shows relative extension combined with LLM, consistent with FMS with normal and LLM components as the 1983 M 6.1 BV EQ. (*e.g.,* Protti and Schwartz, 1994; Boschini et al., 1988).	Yes	–	Yes
CCR-CA interface shows relative compression consistent with the presence of reverse faults as MF, GF and SMF (Denyer et al., 2003).	Yes	Not	Yes
CO-CCR subduction interface reflects LCR consistent with the lack of asperities based on HEQ. (*e.g.,* Protti et al., 1995).	Yes	Not	Yes
Better explanation about the DM of CAFA due to the contribution of the CCR-CAFA collision.	Yes	Not	Yes
Better balance between the HSMRR with the SMAR.	Yes	–	Not

OBS: Observed; CAL: Calculated; ISD: Inter-seismic deformation; RM: Rigid motion; NW: Northwestern; FMS: Focal mechanisms solutions; BF: Barranca fault; TF: Tarcoles fault; LGF: La Garita fault; MF: San Miguel fault; GF: Guapiles fault; SMF: Siquires-Matina fault; VE: Valle de la Estrella; EQ: Earthquake; NE: North-East; LLM: Left Lateral Motion; BV: Buenavista; LCR: Low coupling ratios; HEQ: Historical earthquakes; DM: Driving mechanism; SMAR: Scalar moment accumulation rate; HSMR: Historic seismic moment release rate.

and back arc of the Paleo-volcanic Cordillera de Talamanca estimated in 4–10 mm/yr (Fisher et al., 2004), and the occurrence of slow slip events as it is known in Nicoya Peninsula (*e.g.,* Dixon et al., 2014; Jiang et al., 2012; Outerbridge et al., 2010).

In CCR, along the inland CCR–PM interface (Fig. 5), two segments show the highest slip deficit rates. Historical seismicity records reveal an M 7 earthquake in 1948 close to this interface (Table S5). A weighted average of the slip deficit rate of 3.3 ± 0.3 mm/yr in a locked area of ~1900 km^2 represents a seismic moment accumulation rate of 19.7 ± 1.88 × 10^{16} J/yr (Fig. S29 and Tables S16 and S17), capable of producing M_w 7 earthquakes every 180 ± 16 years. Nevertheless, evidence of faults along these segments are limited (Denyer et al., 2003). In addition, if the M 7 earthquake in 1948 is considered as an asperity released along the PM–CA interface, the second largest earthquake is the M 6.5 earthquake in 1939 (Table S17). The equivalent recurrence period for an M 6.5 earthquake is 65 ± 7 years in a locked

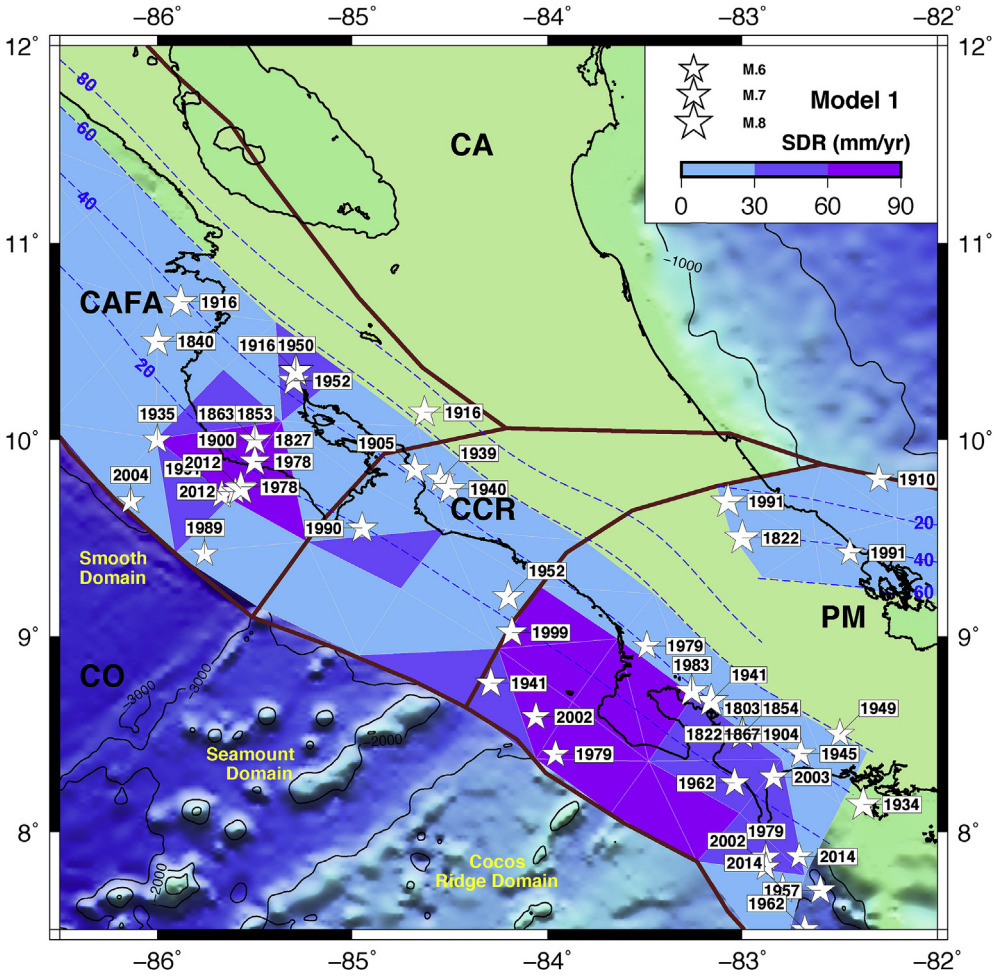

Fig. 4. Slip deficit rates (SDR) and historical seismicity due to the block interaction in subduction interfaces.

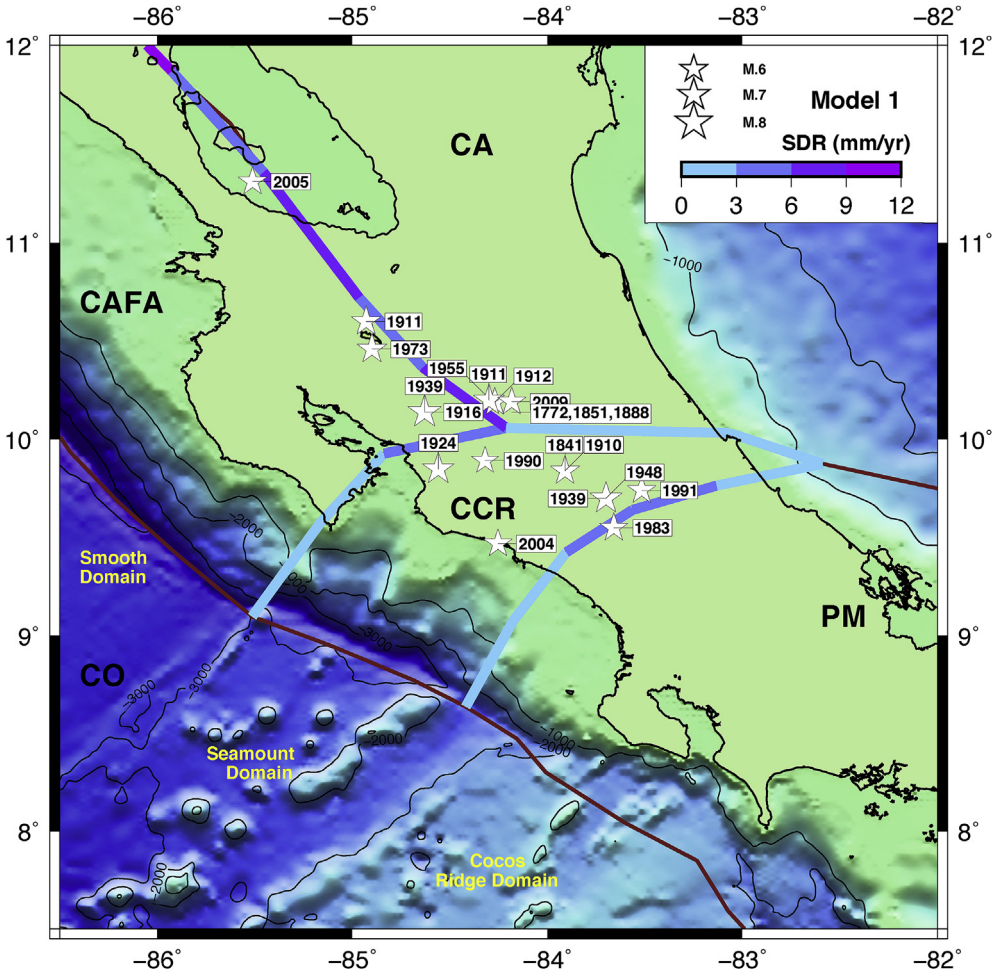

Fig. 5. Slip deficit rates (SDR) and historical seismicity due to the block interaction in inland interfaces.

area of ~900 km^2 and a seismic moment accumulation rate of 9.7 ± 1.08 × 10^{16} J/yr.

The northeastern inland CCR–CAFA interface includes a segment with a slip deficit rate of 3.7 ± 0.2 mm/yr, equal to a seismic moment accumulation rate of 16.8 ± 0.91 × 10^{16} J/yr in a locked area of ~1400 km^2 (Fig. S30 and Tables S18 and S19). If the 1924 M 7.0 Orotina earthquake is adopted as a result of asperity on this interface, we can expect a M$_w$ 7 earthquake every 211 ± 11 years along this interface.

The southeastern segment of the CAFA–CA boundary shows the maximum inland slip deficit rate close to the Metropolitan Area in Costa Rica, reaching a rate of 8.9 ± 0.8 mm/yr (Fig. 5), with an equivalent seismic moment accumulation rate of 33.4 ± 3.0 × 10^{16} J/yr along an interface area of ~1200 km^2 (Fig. S31 and Tables S20 and S21). An earthquake M 7.3 was reported close to this interface in 1939 (Table S21), where we estimated a recurrence period of 299 ± 27 years for this earthquake magnitude. Taking in account that this segment is characterized by an unclear faulting pattern (Denyer et al., 2003; Rodriguez, 2017) and if we assume that the M > 7 earthquakes (in 1916 and 1939) do not correspond to this segment (due to the uncertainties in location and magnitude of historical earthquakes), we can expect an M 6.9 earthquake every 75 ± 7 years in this block interface.

The slip deficit rate determined in the CA–PM subduction interface reflects lower rates in comparison to those obtained along the convergence of CO. The weighted average of slip deficit rate for this zone is 1.6 ± 0.2 mm/yr, but this result is not well constrained by the geodetic observation.

Inversion of slow slip event vectors demonstrated that this kind of events are commonly placed at the entrance of the Nicoya Gulf (depth > 25 km) and off-shore (depth < 20 km) in front of the central coast of NP (Dixon et al., 2014; Jiang et al., 2012; Outerbridge et al., 2010; Voss et al., 2018, 2017). Large events at the entrance of the Nicoya Gulf propagate down-dip of the main earthquake rupture areas, while small off-shore events propagate up-dip to the trench (Dixon et al., 2014). Slow slip events M > 6.5 show recurrence intervals of 20–27 months beneath of NP (*e.g.,* Jiang et al., 2012; Voss et al., 2017) and results of released seismic moment from 2007 to 2012 was 1.6 × 10^{20} J, equivalent to an M 7.5 earthquake (Dixon et al., 2014). This budget of seismic moment released by slow slip events represents a significant amount of energy that can reduce the earthquake potential in locked segments of NP, however the produced slip may also increase the potential in adjacent segments (*e.g.,* Segall et al., 2006). Similar behavior can be occurred beneath OP, but the GNSS network in this peninsula is more recent than in NP, keeping the interest for evaluating the occurrence of this kind of events in OP.

6. Conclusions

We analyzed here the inter-seismic crustal deformation in Costa Rica and the neighborhoods based on the results of the geodetic observations with different coverages of the CCRDB zone. The best results were obtained from the outlined CCRDB zone inferred from Marshall et al. (2000).

Assuming that the seismic moment in the subduction and inland interfaces is accumulated only as elastic strain and is released co-seismically, the resulting seismic moment accumulated rates reflect

capacity for producing M_w 8.1 earthquakes every 225 ± 11 years in southwestern Costa Rica, M_w 7.4 earthquakes every 52 ± 8 years beneath CCR, and M_w 8.3 earthquakes every 128 ± 14 years in southeastern Costa Rica, as the upper limits of the earthquake potential produced by the Cocos Plate convergence. Since no events with such magnitude have ever been recorded in Costa Rica, the model results might be giving an overestimated seismic potential occupied by additional tectonic effects as the post-seismic deformation, plastic deformation, and the occurrence of slow slip events.

We remark that these results may be significantly dependent of the occurrence of slow slip events. These events represent an important amount of energy released along the subduction interface of the Cocos plate beneath Nicoya Peninsula and probably in Osa Peninsula. Slow slip events can reduce the earthquake potential in the locked segments considered in this study, but these events may also increase the potential in adjacent segments.

Along the inland interfaces, the resulted seismic moment accumulated rates reflect upper limits of the earthquake potential up to M_w 7 earthquakes every 180 ± 16 years along the CCR–PM interface, M_w 7 earthquakes every 211 ± 11 years in northeastern CCR–CAFA interfaces, and M_w 7.3 earthquakes every 299 ± 27 years in the southeastern CAFA–CA boundary.

The unclear faulting pattern around the Central Costa Rica block and the uncertainties in location and magnitude of historical earthquakes may disesteem the occurrence of $M > 7$ earthquakes on the inland interfaces. Both historical and current seismicity in Central Costa Rica is very disperse inside the entire CCR block, indicating a very dense array of multiple faults that are probably redistributing strain and strain release over a volume and not necessarily along discrete block boundaries. Nevertheless, the historical seismicity in Costa Rica is still short for disesteeming higher earthquake potential levels along these segments.

Declaration of competing interest

This manuscript has not been published elsewhere and is not under consideration by another journal. We have approved the manuscript and agree with submission to *Journal of South American Earth Sciences*. There are no conflicts of interest to declare.

Appendix A. Supplementary data

Supplementary data to this article can be found online at https://doi.org/10.1016/j.jsames.2019.102375.

References

Adamek, S., Frohlich, C., Pennington, W.D., 1988. Seismicity of the Caribbean- Nazca boundary: constraints on microplate tectonics of the Panama region. J. Geophys. Res. 93, 2053–2075. https://doi.org/10.1029/JB093iB03p02053.

Alonso-Henar, J., Montero, W., Martínez-Díaz, J.J., Álvarez-Gómez, J.A., Insua-Arévalo, J.M., Rojas, W., 2013. The Aguacaliente fault, source of the Cartago 1910 destructive earthquake (Costa Rica). Terra. Nova 25, 368–373. https://doi.org/10.1111/ter.12045.

Altamimi, Z., Collilieux, X., Legrand, J., Garayt, B., Boucher, C., 2007. ITRF2005: a new release of the International Terrestrial Reference Frame based on time series of station positions and Earth Orientation Parameters. J. Geophys. Res. 112, 1–19. https://doi.org/10.1029/2007JB004949.

Altamimi, Z., Collilieux, X., Métivier, L., 2011. ITRF2008: an improved solution of the international terrestrial reference frame. J. Geod. 85, 457–473. https://doi.org/10.1007/s00190-011-0444-4.

Alvarado, G., Morales, L.D., Montero, W., Climent, A., 1988. Aspectos Sismológicos y Morfotectónicos en el Extremo Occidental de la Cordillera Vocánica Central de Costa Rica. Rev. Geol. Am. Cent. 9, 75–98.

Amante, C., Eakins, B.W., 2009. ETOPO1 1 Arc-Minute Global Relief Model: Procedures, Data Sources and Analysis. NOAA Technical Memorandum NESDIS, NGDC-24. 19 pp.

Argus, D.F., Gordon, R.G., DeMets, C., 2011. Geologically current motion of 56 plates relative to the no-net-rotation reference frame. Geochem. Geophys. Geosyst. 12, 1–13. https://doi.org/10.1029/2011GC003751.

Argus, D.F., Heflin, M.B., 1995. Plate motion and crustal deformation estimated with geodetic data from the Global Positioning System. Geophys. Res. Lett. 22, 1973–1976.

Arroyo, I.G., Husen, S., Flueh, E.R., 2014. The seismogenic zone in the Central Costa Rican Pacific margin: high-quality hypocentres from an amphibious network. Int. J. Earth Sci. 103, 1747–1764. https://doi.org/10.1007/s00531-013-0955-8.

Barboza, G., Barrientos, J., Astorga, A., 1995. Tectonic evolution and sequence stratigraphy of the central Pacific margin of Costa Rica. Rev. Geol. Am. Cent. 18, 43–63.

Barckhausen, U., Roeser, H.A., von Huene, R., 1998. Magnetic Signature of the Upper Plate Structures and Subducting Seamounts at the Convergent Margin off Costa Rica, vol. 103. pp. 7079–7093.

Barquero, R., 2009. El Terremoto de Cinchona del 8 de Enero de 2009.

Barquero, R., Rojas, W., 1994. Sismicidad Inducida por el Terremoto de Limón. Rev. Geológica América Cent. esp 111–120.

Bird, P., 2003. An updated digital model of plate boundaries. Geochem. Geophys. Geosyst. 4, 1–52. https://doi.org/10.1029/2001GC000252.

Blewitt, G., Lavallée, D., 2002. Effect of annual signals on geodetic velocity. J. Geophys. Res. Solid Earth 107, ETG 9-1–ETG 9-11. https://doi.org/10.1029/2001jb000570.

Boschini, I., Alvarado, G., Rojas, W., 1988. El terremoto de Buenavista de Pérez Zeledón (Julio 3, 1983): evidencia de una fuente sismogenica intraplaca desconocida en Costa Rica. Rev. Geol. Am. Cent. 8, 111–121.

Bürgmann, R., Thatcher, W., 2013. Space geodesy: a revolution in crustal deformation measurements of tectonic processes. Geol. Soc. Am. 397–430. https://doi.org/10.1130/2013.2500(12.

Camacho, E., Hutton, W., Pacheco, J.F., 2010. A new look at evidence for a wadati-benioff zone and active convergence at the north Panama deformed belt. Bull. Seismol. Soc. Am. 100, 343–348. https://doi.org/10.1785/0120090204.

Camacho, E., Víquez, V., 1993. Historical seismicity of the north Panama deformed belt. Rev. Geol. Am. Cent. https://doi.org/10.15517/rgac.v0i15.13238.

Cho, I., Kuwahara, Y., 2013. Constraints on the three-dimensional thermal structure of the lower crust in the Japanese Islands. Earth Planets Space 65, 855–861. https://doi.org/10.5047/eps.2013.01.005.

DeMets, C., 2001. A new estimate for present-day Cocos-Caribbean plate motion: implications for slip along the Central American volcanic arc. Geophys. Res. Lett. 0, 1–4. https://doi.org/10.1029/2001GL013518.

Denyer, P., Montero, W., Alvarado, G., 2003. Atlas tectónico de Costa Rica, first ed. Editorial de la Universidad de Costa Rica, San José, Costa Rica.

Dixon, T.H., Jiang, Y., Malservisi, R., McCaffrey, R., Voss, N., Protti, M., Gonzalez, V., 2014. Earthquake and tsunami forecasts: relation of slow slip events to subsequent earthquake rupture. Proc. Natl. Acad. Sci. U.S.A. 111, 17039–17044.

Dow, J.M., Neilan, R.E., Rizos, C., 2009. The International GNSS Service in a Changing Landscape of Global Navigation Satellite Systems, vol. 83. Springer-Verlag 2009, pp. 191–198.

Fan, G., Beck, S.L., Wallace, T.C., 1993. The seismic source parameters of the 1991 Costa Rica Aftershock Sequence: evidence for a transcurrent plate boundary. J. Geophys. Res. 98, 15759–15778.

Feng, L., Newman, A.V., Protti, M., Gonzlez, V., Jiang, Y., Dixon, T.H., 2012. Active deformation near the Nicoya Peninsula, northwestern Costa Rica, between 1996 and 2010: interseismic megathrust coupling. J. Geophys. Res. 117, 1–23. https://doi.org/10.1029/2012JB009230.

Fernández, M., 1996. Evaluación del Hipotético Sistema de Falla Transcurrente Este-Oeste de Costa Rica. Rev. Geol. Am. Cent 19/20, 57–74.

Fernández, M., Pacheco, J., Morales, T., 1996. Complejidad de la Estructura Sísmica de la Región Central de Costa Rica según un Análisis Multifractal. Rev. Geol. Am. Cent. 19/20, 29–36.

Fisher, D.M., Gardner, T.W., Marshall, J.S., Sak, P.B., Protti, M., 1998. Effect of subducting sea-floor roughness on fore-arc kinematics, Pacific coast, Costa Rica. Geology 26, 467–470. https://doi.org/10.1130/0091-7613(1998)026<0467:EOSSFR>2.3.CO;2.

Fisher, D.M., Gardner, T.W., Sak, P.B., Sanchez, J.D., Murphy, K., Vannucchi, P., 2004. Active thrusting in the inner forearc of an erosive convergent margin, Pacific coast, Costa Rica. Tectonics 23, 1–13. https://doi.org/10.1029/2002TC001464.

Gilks, W., Richardson, S., Spiegelhalter, D., 1996. Markov Chain Monte Carlo in Practice. Chapman & Hall, London.

Goes, S.D.B., Velasco, A.A., Schwartz, S.Y., Lay, T., 1993. The April 22, 1991, Valle de la Estrella, Costa Rica (Mw = 7.7) earthquake and its tectonic implications: a broadband seismic study. J. Geophys. Res. 98, 8127–8142. https://doi.org/10.1029/93JB00019.

Hanks, T.C., Kanamori, H., 1979. A moment magnitude scale. J. Geophys. Res. 84, 2348–2350.

Hayes, G.P., Moore, G.L., Portner, D.E., Hearne, M., Flamme, H., Furtney, M., Smoczyk, G.M., 2018. Slab2, a comprehensive subduction zone geometry model. Sci. Geophys. https://doi.org/10.1126/science.aat4723.

Jacob, K., Pacheco, J., Santana, G., 1991. Costa Rica earthquake reconnaissance report: seismology and tectonics. Earthq. Spectra 7, 15–33.

Jiang, Y., Wdowinski, S., Dixon, T.H., Hackl, M., Protti, M., Gonzalez, V., 2012. Slow slip events in Costa Rica detected by continuous GPS observations, 2002-2011. Geochem. Geophys. Geosyst. 13, 1–18. https://doi.org/10.1029/2012GC004058.

Kimura, H., Tadokoro, K., Ito, T., 2019. Interplate coupling distribution along the Nankai trough in southwest Japan estimated from the block motion model based on onshore GNSS and seafloor GNSS/A observations. J. Geophys. Res. Solid Earth 124, 1–25. https://doi.org/10.1029/2018JB016159.

Klein, E., Duputel, Z., Zigone, D., Vigny, C., Boy, J.P., Doubre, C., Meneses, G., 2018. Deep transient slow slip detected by survey GPS in the region of Atacama, Chile. Geophys. Res. Lett. 45, 12263–12273. https://doi.org/10.1029/2018GL080613.

Kobayashi, D., LaFemina, P.C., Geirsson, H., Chichaco, E., Abrego, A.A., Mora, H., Camacho, E., 2014. Kinematics of the western Caribbean: collision of the Cocos Ridge and upper plate deformation. Geochem. Geophys. Geosyst. 15, 1671–1683. https://

doi.org/10.1002/2014GC005234.
LaFemina, P., Dixon, T.H., Govers, R., Norabuena, E., Turner, H., Saballos, A., Mattioli, G., Protti, M., Strauch, W., 2009. Fore-arc motion and Cocos Ridge collision in Central America. Geochem. Geophys. Geosyst. 10. https://doi.org/10.1029/2008GC002181.
LaFemina, P.C., Dixon, T.H., Strauch, W., 2002. Bookshelf faulting in Nicaragua. Geology 30, 751–754. https://doi.org/10.1130/0091-7613(2002)030<0751:BFIN>2.0.CO;2.
Linkimer, L., Arroyo, I.G., Alvarado, G.E., Arroyo, M., Bakkar, H., 2018. The National seismological network of Costa Rica (RSN): an overview and recent developments. Seismol. Res. Lett. 89, 392–398. https://doi.org/10.1785/0220170166.
Liu, J., Nordman, D.J., Meeker, W.Q., 2014. The number of MCMC draws needed to compute Bayesian credible bounds. Stat. Prepr. 130, 1–27. https://doi.org/10.1080/00031305.2016.1158738.
Lücke, O.H., Arroyo, I.G., 2015. Density structure and geometry of the Costa Rican subduction zone from 3-D gravity modeling and local earthquake data. Solid Earth 6, 1169–1183.
Marshall, J.S., Fisher, D.M., Gardner, T.W., 2000. Kinematics of diffuse faulting across the western Panama block. Tectonics 19, 468–492.
Metropolis, N., Rosenbluth, A.W., Rosenbluth, M.N., Teller, A.H., Teller, E., 1953. Equation of state calculations by fast computing machines. J. Chem. Phys. 21, 1087–1092. https://doi.org/10.1063/1.1699114.
Montero, L., 1986. Períodos de Recurrencia y Tipos de Secuencias Sísmicas de los Temblores Interplaca e Intraplaca en la Región de Costa Rica. Rev. Geol. Am. Cent. 5, 35–72.
Montero, W., 2001. Neotectónica de La Región central de Costa Rica: frontera Oeste de la Microplaca de Panamá. Rev. Geol. Am. Cent. 24, 29–56.
Montero, W., 1999. El terremoto del 4 de marzo de 1924 (Ms 7,0): ¿Un gran temblor interplaca relacionado al límite incipiente entre la placa Caribe y la microplaca de Panamá? Rev. Geol. Am. Cent. 22, 25–62.
Montero, W., 1994. Neotectonics and related stress distribution in a subduction-collisional zone: Costa Rica. Rev. Geol. Am. Cent. 125–141.
Montero, W., Dewey, J., 1982. Shallow-focus seismicity, composite focal mechanism, and tectonics of the Valle central of Costa Rica. Bull. Seismol. Soc. Am. 72, 1611–1626.
Montero, W., Lewis, J.C., Marshall, J.S., Kruse, S., Wetmore, P., 2013. Neotectonic faulting and forearc sliver motion along the Atirro-Río sucio fault system, Costa Rica, Central America. Bull. Geol. Soc. Am. 125, 857–876. https://doi.org/10.1130/B30471.1.
Montero, W., Paniagua, S., Kussmaul, S., Rivier, F., 1992. Geodinámica Interna de Costa Rica. Rev. Geol. Am. Cent. 14, 1–12.
Montero, W., Rojas, W., 2014. Las Fallas Purires y Picagres, y su relación con la secuencia sísmica se Puriscal de 1990. Rev. Geol. Am. Cent. 50, 39–69.
Moore, G.F., Sender, K.L., 1995. Fracture zone collision along the South Panama margin. Geol. Soc. Am. 295, 201–212. https://doi.org/10.1130/spe295-p201.
Morales, L.D., 1985. Las Zonas Sísmicas de Costa Rica y Alrededores. Rev. Geol. Am. Cent. 3, 69–101.
Nishimura, T., 2014. Pre-, co-, and post-seismic deformation of the 2011 Tohoku-Oki earthquake and its implication to a paradox in short-term and long-term deformation. J. Disaster Res. 9, 1–9.
Norabuena, E., Dixon, T.H., Schwartz, S., DeShon, H., Newman, A., Protti, M., Gonzalez, V., Dorman, L., Flueh, E.R., Lundgren, P., Pollitz, F., Sampson, D., 2004. Geodetic and seismic constraints on some seismogenic zone processes in Costa Rica. J. Geophys. Res. 109, 1–25. https://doi.org/10.1029/2003JB002931.
Okada, Y., 1995. Simulated empirical law of coseismic crustal deformation. J. Phys. Earth 43, 697–713.
Outerbridge, K.C., Dixon, T.H., Schwartz, S.Y., Walter, J.I., Protti, M., Gonzalez, V., Biggs, J., Thorwart, M., Rabbel, W., 2010. A tremor and slip event on the Cocos-Caribbean subduction zone as measured by a global positioning system (GPS) and seismic network on the Nicoya Peninsula, Costa Rica. J. Geophys. Res. 115, 1–17. https://doi.org/10.1029/2009JB006845.
Pacheco, J.F., Quintero, R., Vega, F., Segura, J., Jiménez, W., González, V., 2006. The Mw 6.4 Damas, Costa Rica, earthquake of 20 November 2004: aftershocks and slip distribution. Bull. Seismol. Soc. Am. 96, 1–12. https://doi.org/10.1785/0120050261.
Peterson, E.T., Seno, T., 1984. Factors affecting seismic moment release rates in subduction zones. J. Geophys. Res. 89, 10233–10248.
Protti, M., González, V., Newman, A.V., Dixon, T.H., Schwartz, S.Y., Marshall, J.S., Feng, L., Walter, J.I., Malservisi, R., Owen, S.E., 2013. Nicoya earthquake rupture anticipated by geodetic measurement of the locked plate interface. Nat. Geosci. 7, 117–121. https://doi.org/10.1038/ngeo2038.
Protti, M., Güendel, F., Malavassi, E., 2001. Evaluación del Potential Sísmico de la Peninsula de Nicoya, 1a. ed. Editorial Fundación UNA, Heredia, Costa Rica.
Protti, M., Gündel, F., McNally, K., 1994. The geometry of the Wadati-Benioff zone under southern Central America and its tectonic significance: results from a high-resolution local seismographic network. Phys. Earth Planet. Inter. 84, 271–287. https://doi.org/10.1016/0031-9201(94)90046-9.
Protti, M., McNally, K., Pacheco, J., Gonzalez, V., Montero, C., Segura, J., Brenes, J., Barboza, V., Malavassi, E., Güendel, F., Simila, G., Rojas, D., Velasco, A., Mata, A., Schillinger, W., 1995. The March 25, 1990 (Mw = 7.0, Ml = 6.8), earthquake at the entrance of the Nicoya Gulf , Costa Rica : its prior activity , foreshocks , aftershocks , and triggered seismicity. J. Geophys. Res. 100, 345–358.
Protti, M., Schwartz, S.Y., 1994. Mechanics of back arc deformation in Costa Rica: evidence from an aftershock study of the April 22, 1991, Valle de la Estrella, Costa Rica, earthquake (Mw = 7.7). Tectonics 13, 1093–1107.
Protti, M., Schwartz, S.Y., Zandt, G., 1996. Simultaneous inversion for earthquake location and velocity structure beneath Central Costa Rica. Bull. Seismol. Soc. Am. 86, 19–31.
Quintero, R., Güendel, F., 2000. Stress Field in Costa Rica, vol. 4. Central America, pp. 297–319.
Robert, C., Casella, G., 2004. Monte Carlo Statistical Methods, Second. Springer.
Rodriguez, J., 2017. Potential Sísmico de las Fallas del Cinturón Deformado del Centro de Costa Rica. Universidad de Costa Rica.
Savage, J.C., Simpson, R.W., 1997. Surface strain accumulation and the seismic moment tensor. Bull. Seismol. Soc. Am. 87, 1345–1353.
Segall, P., Desmarais, E.K., Shelly, D., Miklius, A., Cervelli, P., 2006. Earthquakes triggered by silent slip events on Kilauea volcano, Hawaii. Nature 442, 71–74. https://doi.org/10.1038/nature04938.
Sella, G.F., Dixon, T.H., Mao, A., 2002. REVEL: a model for Recent plate velocities from space geodesy. J. Geophys. Res. 107, ETG 11-1–ETG 11-30.
Shen, Z.-K., Jackson, D.D., Ge, B.X., 1996. Crustal deformation across and beyond the Los Angeles basin from geodetic measurements. J. Geophys. Res. 101, 27957–27980.
Silver, E.A., Reed, D.L., Tagudin, J.E., Heil, D.J., 1990. Implications of The north and south Panama thrust belts for the origin of the Panama orocline. Tectonics 9, 261–281.
Suárez, G., Pardo, M., Domínguez, J., Ponce, L., Montero, W., Boschini, I., Rojas, W., 1995. The Limón, Costa Rica earthquake of April 22, 1991: back arc thrusting and collisional tectonics in a subduction environment. Tectonics 14, 518–530. https://doi.org/10.1029/94TC02546.
Tanaka, A., 2004. Geothermal gradient and heat flow data in and around Japan (II): crustal thermal structure and its relationship to seismogenic layer. Earth Planets Space 56, 1195–1199.
Vanness, G., Frohlich, C., Wayne, P., Tosimatu, M., 1984. Seismicity and tectonics of the subducted Cocos plate American and Caribbean plates is probably close. J. Geophys. Res. 89, 7719–7735.
Von Huene, R., Ranero, C.R., Weinrebe, W., Hinz, K., 2000. Quaternary convergent margin tectonics of Costa Rica, segmentation of the Cocos Plate, and Central American volcanism. Tectonics 19, 314–334. https://doi.org/10.1029/1999TC001143.
Voss, N., Dixon, T.H., Liu, Z., Malservisi, R., Protti, M., Schwartz, S., 2018. Do slow slip events trigger large and great megathrust earthquakes? Sci. Adv. 4, 1–5. https://doi.org/10.1126/sciadv.aat8472.
Voss, N.K., Malservisi, R., Dixon, T.H., Protti, M., 2017. Slow slip events in the early part of the earthquake cycle. J. Geophys. Res. Solid Earth 122, 6773–6786. https://doi.org/10.1002/2016JB013741.